TECHNICAL REPORT No. 39

ON THE PARAMETERISATION OF VERTICAL DIFFUSION IN LARGE-SCALE ATMOSPHERIC MODELS

by

M. J. Manton*

*Visiting Scientist on leave from
CSIRO, Australia.

December 1983

C O N T E N T S

Abstract

Vertical diffusion in the ECMWF numerical model is parameterized by a stability-dependent eddy diffusivity. An alternative scheme, in which the eddy diffusivity depends also upon the turbulent kinetic energy, is compared with the ECMWF model. The tests are carried out by integrating a one-dimensional model over a diurnal cycle where there is a transition from stable to unstable conditions. The effects of spatial truncation error on each model are particularly studied.

1. INTRODUCTION

The vertical diffusion of heat, moisture and momentum is represented in the NWP model at the ECMWF by eddy diffusivities that depend upon the local Richardson number (Louis et al. 1981). The diffusivities are chosen to be consistent with the available theory and observations on equilibrium boundary layers and the resulting parameterization is found to yield reasonable results in the ECMWF large-scale model in regions where moist convection is not a dominant process (Tiedtke 1981). Experiments by Miyakoda and Sirutis (1977) suggest that a turbulence-closure scheme based on the work of Mellor and Yamada (1974) can also produce good results in large-scale NWP models. Such schemes, which include the turbulent kinetic energy as a dependent variable, allow turbulence to be advected horizontally and they also allow second-order moments (such as the temperature variance) to be estimated. Thus there may be some advantage in using a higher-order closure scheme to model vertical diffusion in large-scale NWP models. In the present work we describe the development of a turbulent-energy closure scheme for use in the ECMWF large-scale model.

2. TURBULENT-ENERGY MODEL FOR VERTICAL DIFFUSION

The basis of the turbulent-energy model for vertical diffusion is the assumption that the vertical fluxes of scalars, such as heat $\overline{\theta'w'}$ and moisture $\overline{q'w'}$, can be represented by an eddy diffusivity K_Q, where K_Q is proportional to the variance of the vertical velocity $\overline{w'^2}$ (Manton 1980). Thus we take

$$\overline{\theta'w'} = - K_Q \, \partial\theta/\partial z \quad \text{and} \quad \overline{q'w'} = - K_Q \, \partial q/\partial z \, , \tag{2.1}$$

where $K_Q = a_1 \, \overline{w'^2} \, \tau$

In equation (2.1) z is the height above the surface (z=o), θ is the mean potential temperature, q is the mean mass fraction of water vapour, a_1 is a constant and τ is a characteristic time scale for the turbulence; all quantities are ensemble averages.

The time scale τ is an algebraic function of the mean shear and the local flux Richardson number Ri; in particular, we set

$$\tau^{-2} = \left\{(\partial u/\partial z)^2 + (\partial v/\partial z)^2\right\} F(Ri), \qquad (2.2)$$

where (u,v) is the horizontal mean velocity and F is a piecewise linear function of Ri to be determined. The variance $\overline{w'^2}$ is taken to be an algebraic function of the turbulence kinetic energy E, while E is found by simplifying the full turbulent energy equation

$$\frac{dE}{dt} + \overline{u'w'}\,\frac{\partial u}{\partial z} + \overline{v'w'}\,\frac{\partial v}{\partial z} + \frac{1}{2}\frac{\partial}{\partial z}\left\{\overline{w'(u'^2 + v'^2 + w'^2}\right\}$$

$$+ \frac{1}{\rho}\frac{\partial}{\partial z}\,\overline{(p'w')} + (g/\rho)\,\overline{\rho'w'} = \nu(\overline{u'\nabla^2 u'} + \overline{u'\nabla^2 v'} + \overline{w'\nabla^2 w'}) \ , \qquad (2.3)$$

where t is time; ρ', p', u' and v' are the fluctuations in density, pressure and velocity about their mean values; ρ is the mean density; g is the gravitational acceleration and ν is kinematic viscosity of air. Horizontal gradients in (2.3) are assumed to be negligible in comparison with vertical gradients, except in the advection terms.

In order to estimate the relationship between $\overline{w'^2}$ and E, we consider the equation for the anisotropic components of the velocity covariance tensor S_{ij}, where in tensor notation

$$S_{ij} = \overline{u'_i\,u'_j} - \frac{1}{3}\,\overline{u'_m\,u'_m}\,\delta_{ij} \qquad (2.4)$$

and $(u'_1, u'_2, u'_3) \equiv (u', v', w')$. Under the assumption that the anisotropy of the covariance is maintained primarily by the working of the turbulent stresses against the mean strain rate, it is found (Manton 1979) that the covariance is given by the equation

$$\overline{u_i' u_j'} \frac{\partial u_k}{\partial x_j} + \overline{u_k' u_j'} \frac{\partial u_i}{\partial x_j} - \frac{2}{3} \overline{u_m' u_j'} \frac{\partial u_m}{\partial x_j} \delta_{ik}$$

$$+ (a_2/\tau) \left(\overline{u_i' u_k'} - \frac{1}{3} \overline{u_m' u_m'} \delta_{ik}\right) = 0 \qquad (2.5)$$

where $(x_1, x_2, x_3) \equiv (x, y, z)$ and a_2 is a constant. The last term in (2.5) represents the redistribution of turbulent energy among the x, y and z components by the working of the turbulent pressure fluctuations against the turbulent strain rate. Equation (2.5) is an algebraic set for the six covariance components; in particular, we find that

$$\overline{u'w'} = - K_m \partial u/\partial z, \quad \overline{v'w'} = - K_m \partial v/\partial z, \qquad (2.6)$$

$$\overline{w'^2} = \frac{2}{3} E/\left\{1 + \frac{2}{3} \left(\frac{\tau}{a_1}\right)^2 \left[\left(\frac{\partial u}{\partial z}\right)^2 + \left(\frac{\partial u}{\partial z}\right)^2\right]\right\} ,$$

where $E = \frac{1}{2} (\overline{u'^2} + \overline{v'^2} + \overline{w'^2})$ and $K_m = \overline{w'^2} \tau/a_1$.

Equation (2.6) allows the diffusivity K_Q in (2.1) and the mechanical production terms in (2.3) to be specified in terms of E and the mean gradients of θ, q and velocity. In the absence of condensation the buoyancy flux term in (2.3) is found from (2.1) and the equation of state to be given by

$$(g/\rho) \overline{\rho'w'} = K_Q B , \qquad (2.7)$$

where $B = g\left[\frac{1}{\theta} \frac{\partial \theta}{\partial z} + (R_v/R_a - 1) \frac{\partial q}{\partial z}\right]$,

R_v and R_a are the gas constants for water vapour and dry air. The right-hand side of (2.3) accounts for the molecular diffusion and the dissipation of turbulent energy. The former effect is negligible while dissipation is assumed to occur with a time scale of order τ; that is, we take

$$\nu (\overline{u'\nabla^2 u'} + \overline{v'\nabla^2 u'} + \overline{w'\nabla^2 w'}) = - a_3 E/\tau , \qquad (2.8)$$

where a_3 is a constant. The transport of turbulent energy by turbulent fluctuations in (2.3) is modelled by the equation

$$\frac{1}{2}\,\overline{w'\,(u'^2 + v'^2 + w'^2)} + \overline{p'w'}/\rho = -\,K_Q\,\frac{\partial E}{\partial z} - a_4(\overline{w'^2})^{\frac{1}{2}}\,\tau\,K_Q B\ , \qquad (2.9)$$

where a_4 is a constant. The first term on the right-hand side of (2.9) accounts for transport down the gradient of E. The second term is needed for statically unstable cases (B<0) when the vertical transport of energy may be supported by hydrostatic pressure fluctuations (Manton 1980).

Putting (2.6) - (2.9) into (2.3) we find that the behaviour of the turbulent energy E may be modelled by the equation

$$\frac{dE}{dt} = \phi E + \frac{1}{\rho}\frac{\partial}{\partial z}\left(\rho\,K_Q\,\frac{\partial E}{\partial z}\right) + \frac{1}{\rho}\frac{\partial}{\partial z}\left(\rho\psi E\right)\ , \qquad (2.10)$$

where $\phi = \left\{\alpha_2\,(1-Ri)/(a_2F) - a_3\right\}/\tau\ ,$

$$\psi = a_1 a_4\,\alpha_2^{3/2}\,\tau^2\,BE^{\frac{1}{2}}\ ,$$

$$K_Q = a_1\,\alpha_2\,E\,\tau\ ,$$

$$\alpha_2 = 1/\left\{\frac{3}{2} + 1/(a_2^2\,F)\right\}$$

$$Ri = a_1\,a_2\,B/\left\{\left(\frac{\partial u}{\partial z}\right)^2 + \left(\frac{\partial v}{\partial z}\right)^2\right\}$$

The first term on the right-hand side of (2.10) represents the net rate of production of turbulent energy; the three terms in ϕ are the mechanical generation by the shear stress, the suppression by the mean stratification and the dissipation by viscous forces. The last two terms of (2.10) represent the turbulent transport given by (2.9).

The function F(Ri) and the constants a_1, a_2, a_3 and a_4 are found by comparing the solutions of (2.10) with the observed behaviour of an equilibrium surface layer. Then the fluxes of heat, moisture and momentum can be estimated from (2.1) and (2.6) in terms of the mean variables E, u, v, θ and q.

3. EQUILIBRIUM SURFACE LAYER

We consider an equilibriumm surface layer in which $dE/dt = 0$, $\underset{\sim}{u} = (u,o,o)$, $q = 0$ and the fluxes $\overline{u'w'}$ and $\overline{\theta'w'}$ are constants. In neutral conditions ($Ri = 0$) the turbulent time scale is given by the mean shear and so we take

$$F = 1 \text{ at } Ri = 0 \; . \tag{3.1}$$

Observations, summarized by Mellor and Yamada (1974), show that the shear stress in neutral conditions is given by

$$-\overline{u'w'}/E = 0.32 \tag{3.2}$$

Putting (3.2) into (2.6) and (2.10) we find a quadratic equation for a_2. The appropriate root of the equation is chosen so that the stresses $\overline{w'^2}$ and $\overline{v'^2}$ from (2.5) are consistent with the observations discussed by Mellor and Yamada. It is finally found that

$$a_2 = 1.69 \text{ and } a_3 = 0.32 \; . \tag{3.3}$$

We also take K_Q equal to K_m (Louis et al 1981) and then (2.1) and (2.10) imply that

$$a_1 = 0.59 \; . \tag{3.4}$$

We note that, because the assumed behaviour of the anisotropic component of the velocity covariance (2.5) is independent of the buoyancy flux, the diffusivities of heat and momentum are equal for all values of Ri in the present parameterization.

For slightly stable conditions we assume that E is independent of height and that the gradients of u and θ are constant. Then (2.10) reduces to $\phi = 0$ and the normalized time scale F in (2.2) is found to be a linear function of Richardson number; in particular, for $0 < Ri < Ri_{cr}$

$$F = 1 - 1.23 \; Ri \; , \tag{3.5}$$

where Ri_{cr} is the critical Richardson number beyond which turbulent is

suppressed. Observations by Businger et al (1971) suggest that Ri_{cr} is equal to 0.21. Assuming that the Brunt-Vaisala frequency yields an appropriate time scale for suppressed turbulence we see from (3.5) that for Ri>0.21

$$F = 3.53\ Ri\ . \tag{3.6}$$

As $Ri \to -\infty$ the turbulent time scale should be independent of the mean shear and so for Ri<0 we take

$$F = 1 - a_5\ Ri \tag{3.7}$$

To determine a_5 we use the observation of Wyngaard and Coté (1971) that the rate of dissipation of turbulent energy is about 35% of the rate of production by buoyancy forces in free convection, i.e. as $Ri \to -\infty$. Thus it is found from (2.7) and (2.10) that

$$a_5 = 0.43\ . \tag{3.8}$$

The last term in (2.10) is introduced so that the turbulent transport term can act as an energy sink in free convection. The term is irrelevant in stable conditions when the atmosphere supports waves rather than convective thermals and hence a_8 is set equal to zero for Ri>0. The value of a_8 for unstable conditions is calculated from (2.10) using the observation of Wyngaard et al (1971) that

$$\overline{w'^2} = 3.6\ (\kappa g\ \overline{\theta' w'}\ z/\theta)^{2/3}\ , \tag{3.9}$$

where κ is the von Karman constant (0.4). We therefore take

$$a_4 = \begin{cases} 0, & Ri>0\ . \\ \\ 1.79, & Ri\leq 0\ . \end{cases} \tag{3.10}$$

Equations (3.3) - (3.8) and (3.10) can be put into the energy equation (2.10) in order to predict the behaviour of E as a function of time for all mean

stability conditions. The mean stability parameter B in (2.7) does not account for the effects of cloud.

4. DISCRETIZATION OF TURBULENT ENERGY EQUATION

The discretization and numerical solution of (2.10) is similar to the methods used for the primary vaariables in the ECMWF large-scale model (Louis 1981). None of the tests described in the present report account for the advection of E. The left-hand side of (2.10) is therefore reduced to a simple time derivative and we consider the solution of a parabolic equation for vertical diffusion using a centred time difference and an implicit representation of E on the right-hand side of (2.10).

The equation of state and the hydrostatic equation together imply that

$$\frac{1}{\rho}\frac{\partial}{\partial z} = -\frac{g}{p_s}\frac{\partial}{\partial \sigma} , \qquad (4.1)$$

where $\sigma = p/p_s$, p is the pressure and p_s is the surface pressure. Thus (2.10) reduces to the equation

$$\frac{\partial E}{\partial t} - \phi E = G , \qquad (4.2)$$

where

$$G = \frac{\partial}{\partial \sigma}\left\{\left(\frac{\sigma g}{RT}\right)^2 K_Q \frac{\partial E}{\partial \sigma}\right\} - \frac{\partial}{\partial \sigma}\left\{\left(\frac{\sigma g}{RT}\right) \psi E\right\} ,$$

$$T = \theta \sigma^{Ra/Cpa} ;$$

T is the air temperature, Cpa is the specific heat at constant pressure for dry air. The discretization of the right-hand side of (4.2) is taken to be

$$2\Delta t\, G_k = A_k (E_{k+1}^{\tau+1} - E_k^{\tau+1}) - C_k (E_k^{\tau+1} - E_{k-1}^{\tau+1})$$
$$- M_k (E_{k+1}^{\tau+1} + E_k^{\tau+1}) + N_k (E_k^{\tau+1} - E_{k-1}^{\tau+1}) , \qquad (4.3)$$

where

$$A_k = (\sigma g/RT)^2_{k+\frac{1}{2}} (2\Delta t\, K_{Qk+\frac{1}{2}}/\Delta\sigma_{k+\frac{1}{2}}\Delta\sigma_k),$$

$$C_k = A_{k-1}\,\Delta\sigma_{k-1}/\Delta\sigma_k,$$

$$M_k = (\sigma g/RT)_{k+\frac{1}{2}}\,(2\Delta t\,\psi_{k+\frac{1}{2}}/2\Delta\sigma_k)\ ,$$

$$N_k = M_{k-1}\,\Delta\sigma_{k-1}/\Delta\sigma_k\ ,$$

where Δt is the time step, $\Delta\sigma_k$ is the increment in σ at level k (k=1,...,N), E_k^τ is the value of E at time $\tau\Delta t$ and level k. The non-linear coefficients A_k, C_k, M_k and N_k are evaluated at time $(\tau-1)\Delta t$.

The discretization of the ϕ-term in (4.2) must be handled carefully because that term tends to dominate the equation. The coefficient of E on the right-hand side of (4.2) is approximated by A_k which is of order $\Delta t\ K_Q/(\Delta z)^2$, where Δz is an increment in z. Typical values are Δt = 900 s, K_Q = 1 $m^2\ s^{-1}$ and Δz = 300 m for the ECMWF model, and so the coefficient A_k is of order 10^{-2}. On the other hand ϕ scales with $1/\tau$ and the turbulent time scale is generally of order 500 s. Thus the coefficient $\phi\Delta t$ tends to be greater than unity. Moreover the coefficient is positive in unstable conditions and negative in stable conditions. We therefore take the formal solution of (4.2); namely,

$$\frac{\partial}{\partial t}\left\{E\exp\left(-\int \phi dt\right)\right\} = G\exp\left(-\int\phi\ dt\right)\ .$$

The total discretization of (4.2) is then given by

$$E_k^{\tau+1} = \gamma_k\,E_k^{\tau-1} + 2\Delta t\ G_k\ , \qquad (4.4)$$

where

$$\gamma_k = \zeta_k\,\beta_{k-\frac{1}{2}} + (1-\zeta_k)\,\beta_{k+\frac{1}{2}}\ ,\quad \zeta_k = \Delta\sigma_{k+\frac{1}{2}}/2\Delta\sigma_k\ ,$$

$$\beta_{k+\frac{1}{2}} = \begin{cases} 1 + 2\Delta t\ \phi_{k+\frac{1}{2}}\ , & \phi_{k+\frac{1}{2}} \geq 0\ . \\ 1/\ (1 - 2\Delta t\ \phi_{l+\frac{1}{2}})\ , & \phi_{k+\frac{1}{2}} < 0\ . \end{cases}$$

The function $\beta_{k+\frac{1}{2}}$ is an approximation to $\exp(2\Delta t\ \phi_{k+\frac{1}{2}})$, and γ_k accounts for an irregular spatial grid.

The tridiagonal system (4.3) - (4.4) is solved for k=1,...,N with $E_N^{\tau+1}$ specified and the boundary condition of zero flux at the top (i.e. $C_o = N_o = 0$). Because the generation term dominates the turbulence equation, E tends rapidly to its equilibrium value and so the initial distribution of E is not critical to the ultimate solution. We therefore set the initial value of E at time t=0 such that

$$E_k^o = E_{min} \quad , \quad k=1,\ldots,N, \tag{4.5}$$

where E_{min} is usually 0.01 $m^2\ s^{-2}$. The exponential behaviour of (3.2) causes E to decrease rapidly in regions where $Ri > Ri_{cr}$. Because equation (4.4) is homogeneous, the value of $E_k^{\tau-1}$ is replaced by max (E_{min}, $E_k^{\tau-1}$) so that E_k^{τ} can grow locally when instability occurs.

5. SURFACE BOUNDARY CONDITIONS

The value of the turbulent kinetic energy E is specified at the lowest grid point (k=N) through use of the equilbrium surface layer observations discussed in Sect.3. For neutral conditions the mean velocity $\bar{u}$ is given by the logarithmic profile

$$\bar{u} = (u_*/\kappa) \log (z/z_o) \ , \tag{5.1}$$

where z_o is the specified roughness height of the surface and u_* is the friction velocity. Using (3.2) and (5.1) we therefore find the boundary value of E for Ri = 0 to be

$$E_N = 3.13\ C_D\ (u_N^2 + v_N^2) \ , \tag{5.2}$$

where $C_D = \{\kappa/\log (z_N/z_o)\}^2$,

z_N is the height of level k=N above the surface, and (u_N, v_N) is the velocity at k=N. Turbulence is found to be reduced with increasing Richardson number and it is suppressed when Ri is greater than the critical value Ri_{cr}. Thus, for Ri>0, we take

$$E_N = \max \left\{ E_{min},\ 3.13\ C_D\ (u_N^2 + v_N^2)\ (1 - Ri_N/Ri_{cr}) \right\} \qquad (5.3)$$

where Ri_N is the bulk Richardson number of the layer from the surface to level k=N.

To determine E_N in unstable conditions the observed result for $\overline{w'^2}$ is used in the model equations. Then integration of (2.1) for the virtual potential temperature profile yields an estimate of the enhancement of E due to a superdiabatic surface layer. It is finally found that for Ri<0

$$E_N = 3.13\ C_D\ (u_N^2 + v_N^2) + 3.02\ (z_o/z_N)^{1/3}\ gz_N\ (\theta_{v,s} - \theta_{v,N})/\theta_s, \qquad (5.4)$$

where θ_v is the virtual potential temperature.

The difference equation (4.4) for the turbulent energy E_k^τ is solved with the initial condition (4.5) and the boundary conditions (5.3) - (5.4). The complete system of equations for the mean temperature T, water mass frction q and velocity (u,v) is closed by specifying the diffusivities of heat $K_{Q,N+\frac{1}{2}}$ and momentum $K_{M,N+\frac{1}{2}}$ in the surface layer. Although the present parameterization has K_Q equal to K_M within the bulk of the atmosphere, detailed observations suggest that this approximation is valid in the surface layer under only neutral stability conditions. For most of the computations in the present work we therefore take the surface values of K_Q and K_M used in the ECMWF large-scale model (Louis et al 1981). However, some calculations are carried out using the simple approximation

$$K_{M,N+\frac{1}{2}} = K_{Q,N+\frac{1}{2}} = \begin{cases} \max\left\{0, C_D z_N (u_N^2+v_N^2)^{\frac{1}{2}}\ (1-Ri/Ri_{cr})\right\}\ , & Ri>0\ . \\ \\ C_D z_N\ (u_N^2 + v_N^2)^{\frac{1}{2}}, & Ri\leq 0\ . \end{cases} \qquad (5.5)$$

6. SLIGHTLY STABLE BOUNDARY LAYER

Tiedtke (1981) shows that the ECMWF parameterization of the eddy diffusivities yields a good approximation to the "Leipzig" wind profile (Mildner 1932) observed in slightly stable conditions. It is appropriate to test the present turbulence scheme on the same data set. The ECMWF grid-point model is run in its one-column mode, in which the adiabatic terms of the equations of motion are specified and the equations reduce to a one-dimensional set for the vertical distribution of the dependent variables. For the present test the temperature T and moisture q profiles are fixed and the horizontal pressure gradients in the momentum equations are specified. The distribution of grid-point σ-levels in the vertical is given by

$$\sigma_k = 0.75\ j + 1.75\ j^3 - 1.5\ j^4\ , \qquad (6.1)$$

where $j = (2k-1)/2N$ and $k=1,\ldots,N$. The number of vertical grid points N is set equal to 15 so that the observed boundary layer occupies the lowest three levels. The initial velocity profile is set at the observed values and the equations are integrated with a time step of 900 s.

Figure 1 shows that a steady solution is obtained after about 12 h of integration. We note that a steady solution is not readily attained unless the parameter a_8 in (2.9) is equal to zero for stable conditions, as discussed in Sect.3. In Fig.2 the computed steady velocity profile is compared with the derived profile of Carson and Smith (1973) and with that predicted by the ECMWF parameterization. The low level wind is seen to be overestimated by the E-model and this is reflected in the surface stress being 0.54 N m^{-2} compared with the observed value of 0.47 N m^{-2}. (Another analysis of the Leipzig data by Lettau (1950) yields a surface stress of 0.54 N m^{-2}).

We find that essentially the same result is obtained if the boundary value of K_m is given by the simple representation (5.5), rather than the detailed ECMWF

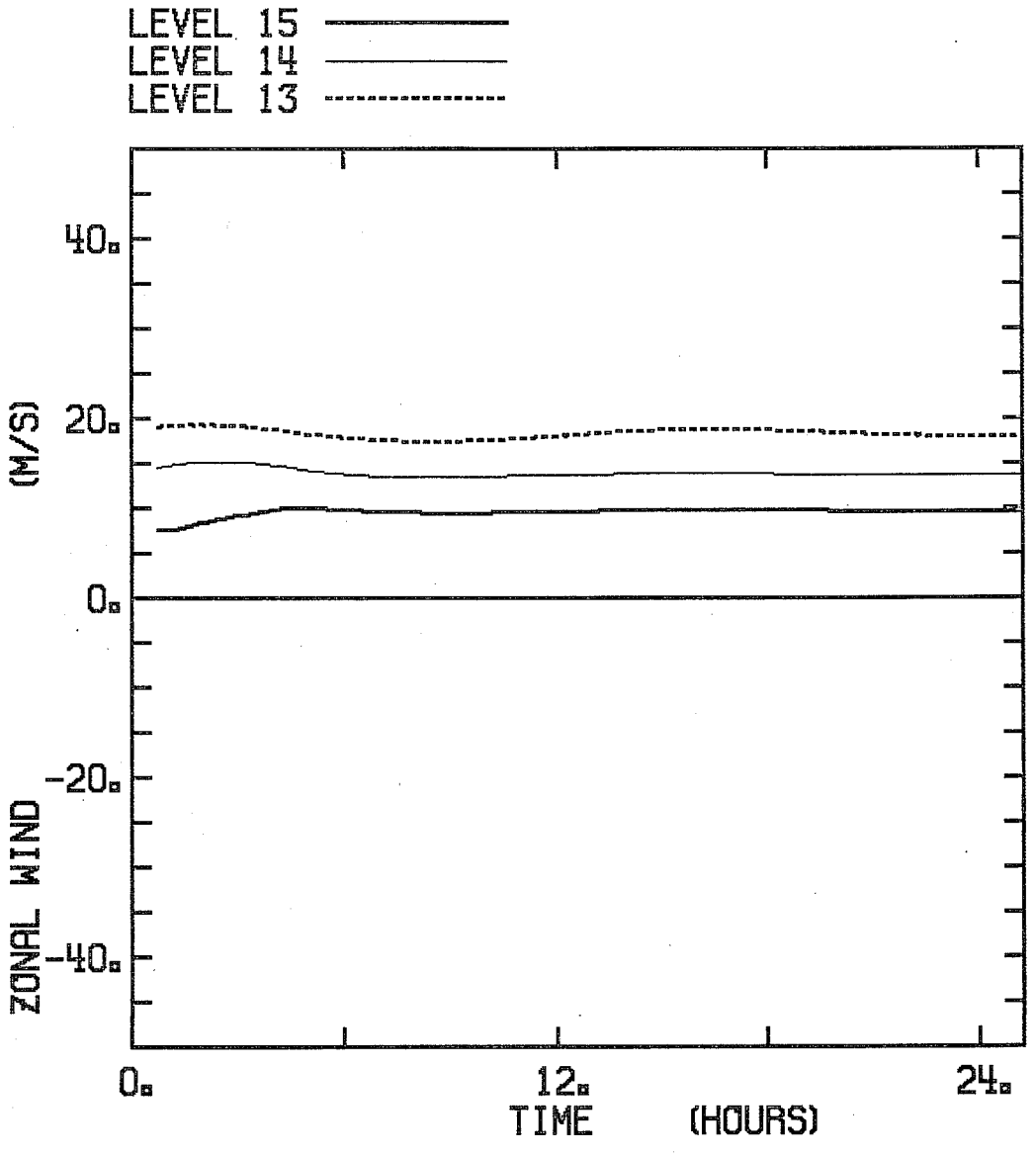

Fig. 1 Temporal variation of the zonal wind component at levels 13, 14 and 15 (σ = 0.914, 0.967, 0.996) for Leipzig profile using E - model for turbulent diffusion.

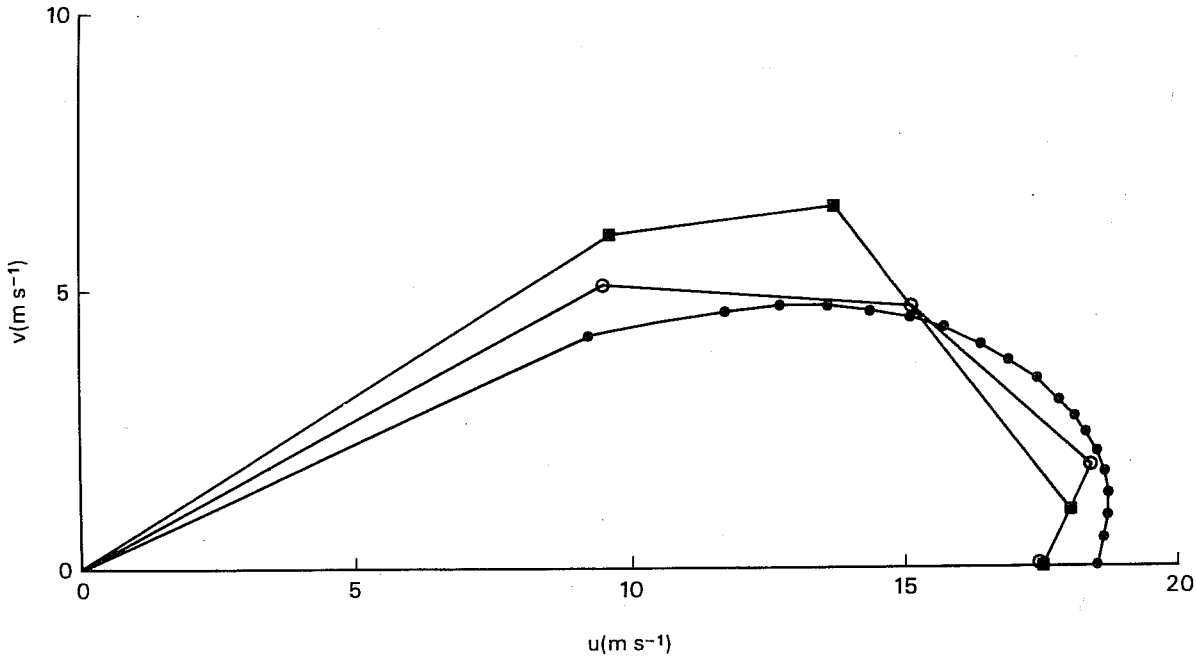

Fig. 2 Steady velocity profile for Leipzig conditions; ● Carson and Smith (1973); o ECMWF model; ■ E-model.

version. However, this result is expected because the surface layer in this case is near neutral stability where the two representations are equivalent.

7. DIURNAL VARIATION OF THE BOUNDARY LAYER

In order to compare the behaviour of the ECMWF turbulence scheme with the present E-model in unstable atmospheric conditions we consider a 24-hour integration that approximates the observed diurnal changes during Day 33 of the Wargara experiment (Clarke et al 1971). A one-dimensional numerical model, described in Appendix A, is used so that the vertical grid spacing can be readily altered. The model does not include a surface parameterization and so the surface temperature T_s is a specified function of time. Earlier tests with the full ECMWF one-column model show that a suitable function for T_s in degrees K is

$$T_s = \begin{cases} 276 \ , \quad 0<t<8 \text{ hrs} \ . \\ 276 + 3.455\ (t-8), \quad 8<t<13.5 \text{ hrs} \ . \\ 295 - 1.810\ (t-13.5) \ , \quad 13.5<t<24 \text{ hrs} \ . \end{cases} \tag{7.1}$$

Equation (7.1) represents the effects of the diurnal variation of the radiation flux at the surface. The surface wetness W_s is fixdd at 0.05. The initial profiles of u,v,T and q are shown in Table 1. The geostrophic wind (u_g, v_g) is set equal to the initial wind velocity. Advection effects are neglected.

The ECMWF operational model uses the standard vertical grid (6.1) with N=15 and a typical time step Δt is 900 s. Figure 3 compares the results of the ECMWF model with the E-model for these standard conditions. It is clear from the behaviour of the water mass fraction q that, when convection begins after about 10 hrs, the E-model generates a deeper and more uniform mixed layer than that of the ECMWF model. The entrainment of warm air causes the potential

Table 1 Initial profiles for Wangara conditions

p(mb)	u(m s^{-1})	v(m s^{-1})	T(K)	q(g kg^{-1})
26	5	0	216.1	0.001
78	7	0	216.2	0.001
135	10	0	216.2	0.001
197	15	0	216.2	0.001
266	20	0	223.2	0.001
341	25	0	234.2	0.01
423	25	0	244.2	0.01
511	23	0	253.2	0.01
601	20.4	0	260.9	0.05
692	14.8	0	267.6	0.2
781	10.1	0	272.4	0.7
863	6.2	0	272.5	2.2
934	6.0	0	277.6	3.3
987	6.0	0	281.8	4.0
1017	6.0	0	281.6	4.2

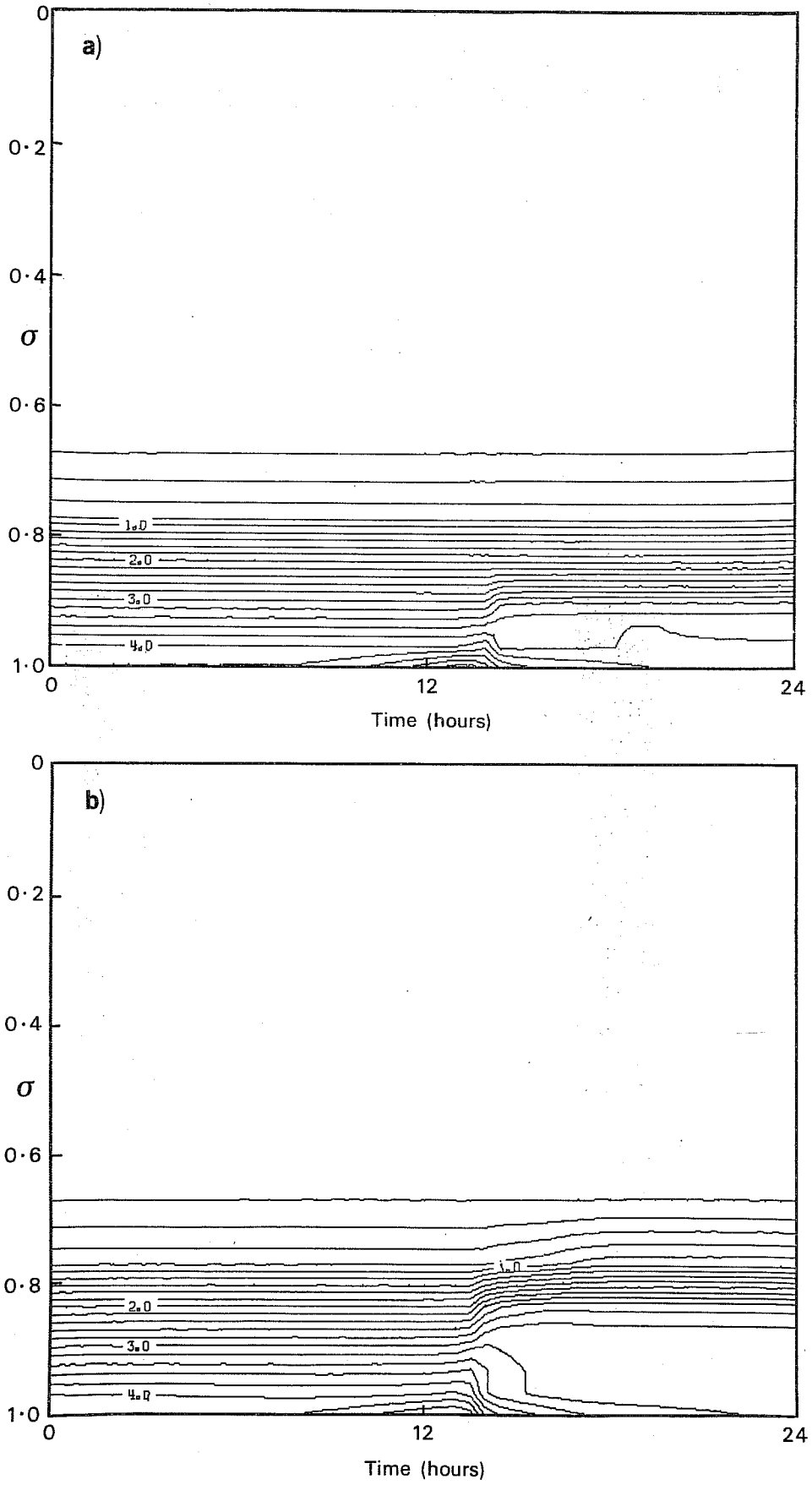

Fig. 3 Temporal variation of the water mass fraction q for Wangara conditions for ECMWF grid with N=15 and Δt=900 s; (a) ECMWF model; (b) E-model.

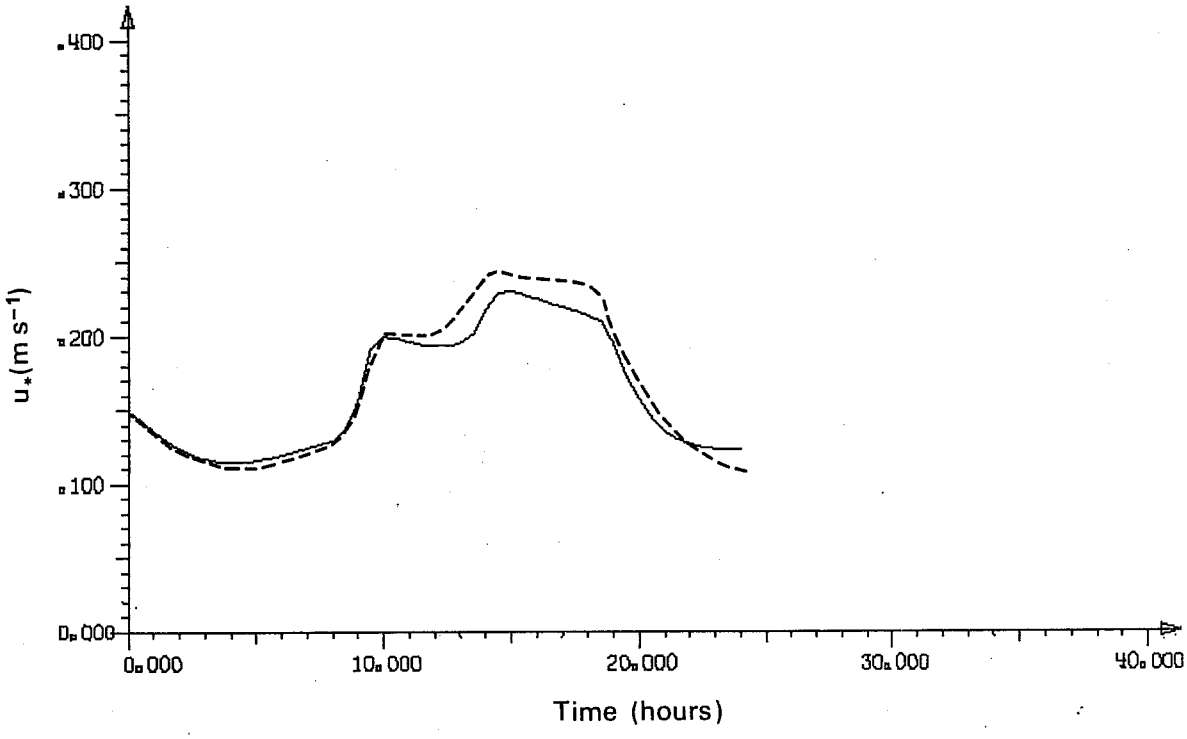

Fig. 4 Variation of friction velocity u_* with time for Wangara conditions for ECMWF grid with N=15 and Δt=900s; —— ECMWF model, ---- E-model.

temperature θ of the E-model mixed layer to be 0.5 K higher than that in the ECMWF model, and consequently the net transfer of sensible heat from the surface to the atmosphere is only 1.58 MJ m^{-2} for the E-model compared with 1.65 MJ m^{-2} for the ECMWF model. However, the transfer of total (sensible plus latent) heat is almost identical for the two cases: 2.11 MJ m^{-2} for the E-model and 2.08 MJ m^{-2} for the ECMWF model. The difference in latent heat fluxes arises because entrainment causes q in the E-model mixed layer to be about 0.7 g kg^{-1} less than that for the ECMWF model.

It is clear from Fig.4 that the predicted values of the friction velocity u_* are comparable for the two models. On the other hand the dissipation of kinetic energy for the ECMWF model is 0.058 MJ m^{-2}, which is about three times the dissipation of the ECMWF model (0.022 MJ m^{-2}). The increased dissipation of the ECMWF model is associated with friction at high levels in the atmosphere, where weak inertial oscillations are established.

If the surface values of K_Q and K_M are given by the simple equation (5.5) rather than the ECMWF representation then the E-model still produces a mixed layer comparable with that shown in Fig.3b. However, the surface transports of heat and moisture are grossly different, primarily because of the behaviour of (5.5) in strongly stable conditions. The diffusivity for momentum K_M approaches zero with increasing Ri much more rapidly than does K_M in the ECMWF formulation. If the ECMWF scheme, which is based on studies of the surface layer, is correct then u_* is markedly underestimated by (5.5) during the night and the total dissipation of kinetic energy is only 0.016 MJ m^{-2} over 24 hours. On the other hand the ECMWF parameterization has K_Q decreasing more rapidly with Ri than does K_M. This process allows a substantial shear stress to be maintained while the fluxes of heat and moisture are negligible in strongly stable conditions. Since (5.5) has K_Q equal to K_M we find that

there is considerable flux of heat and moisture to the surface during night-time and so the net transports of sensible and latent heat are found to be only 1.24 and 0.40 MJ m^{-2} over the 24-hour period.

8. TRUNCATION ERROR IN VERTICAL DIFFUSION

The differences found in Sect.7 between the ECMWF model and the E-model are caused either by the physical differences in the turbulence parameterizations or by differing effects of truncation error. To estimate the effects of truncation error the models are integrated at increased spatial and temporal resolution. Fig.5 shows the variation of water mass fraction q with time for each model with a 90-level uniform grid and a time step Δt of 225 s. (Increasing the number of levels to 145 or decreasing Δt to 112.5 s has little effect on the results. We note that increasing the resolution on the ECMWF grid (6.1) does not produce convergent results). It is apparent that not only do the models produce different solutions but also each suffers from truncation error when the usual ECMWF resolution is used.

Table 2 lists the values of u,v,θ and q in the mixed layer at t = 18 hr for each model; p_o is the pressure at the top of the mixed layer. The E-model is found to produce a deeper and more uniform mixed layer than the ECMWF model. Thus the extra entrainment of warm dry air causes the mixed layer to be warmer and drier. On the other hand the velocity is similar for each case because the initial profile is essentially uniform up to 860 mb. Both models produce a sharp interface at the top of the mixed layer.

Although the mixed-layer properties differ, the net flux of heat from the surface into the atmosphere is equivalent. The sensible heat transfer is 1.71 MJ m^{-2} and the latent heat transfer is 0.41 MJ m^{-2} for the ECMWF model over 24 hrs while the corresponding values for the E-model are 1.70 and 0.44 MJ m^{-2}.

Table 2 Mixed-layer properties for Wangara conditions at t=18 hrs

	u_o(m s^{-1})	v_o(m s^{-1})	θ(K)	q_o(g kg^{-1})	p_o(mb)
ECMWF	5.80	-0.53	285.75	3.44	868
E-model	5.95	-0.56	286.11	3.16	845

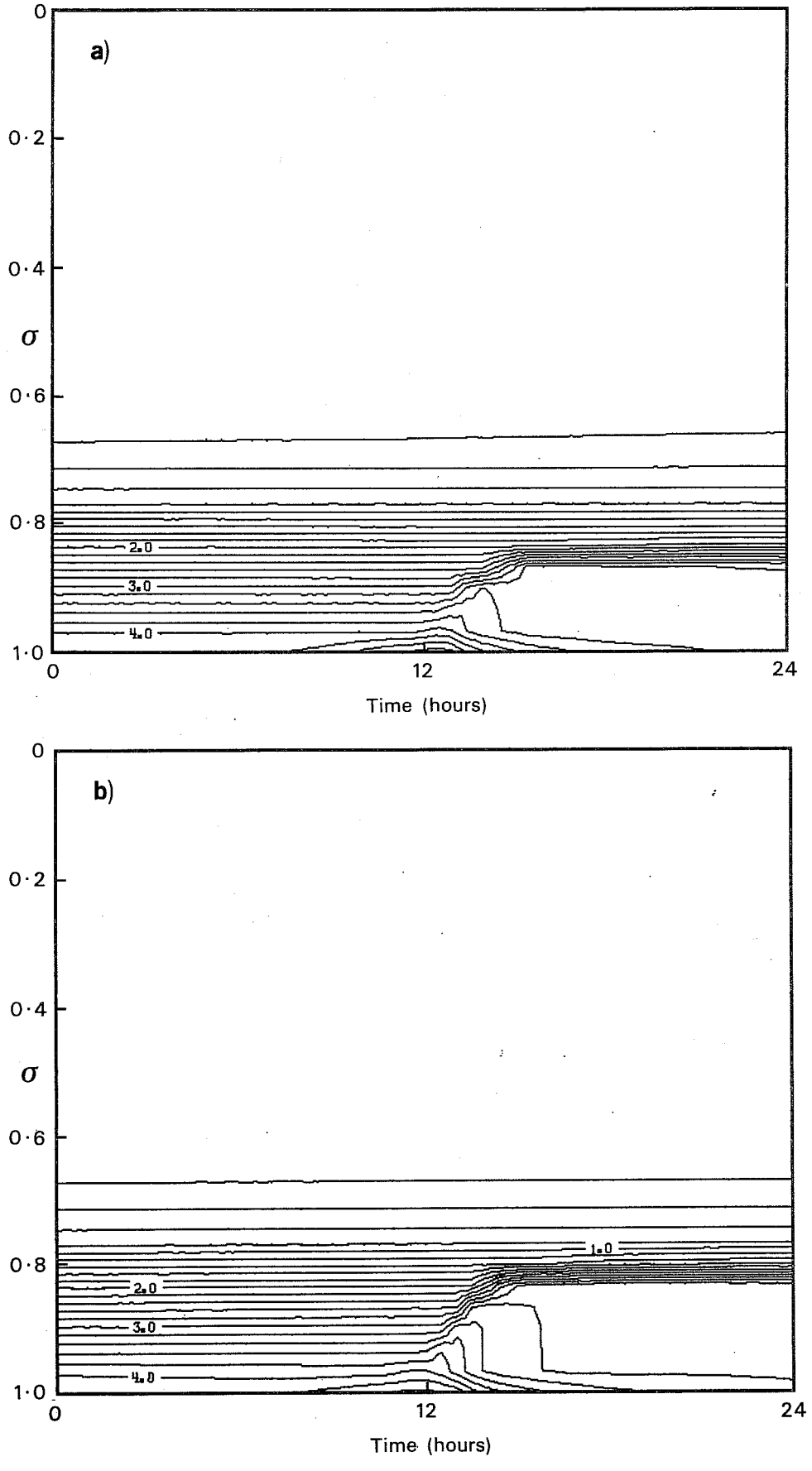

Fig. 5. Temporal variation of water mass fraction q for Wangara conditions for uniform grid with N=90 and Δt=225s; (a) ECMWF model; (b) E-model.

The value of the friction velocity u_* is also similar over the 24-hr period. These results imply that the main impedance in the transfer of momentum, heat and moisture between the troposphere and the surface is in the atmospheric surface layer. Using the same parameterization for the eddy diffusivity in the surface layer produces similar results in the overall budgets of heat and moisture for both models. The kinetic energy budget is different for each model because the ECMWF model dissipates much more energy than the E-model; in particular, the net dissipation is 0.054 MJ m^{-2} for the former and 0.019 MJ m^{-2} in the latter over 24 hrs. In both cases the net kinetic energy increases owing to the work done by the pressure gradient being slightly greater than the dissipation. At t=24 hrs the increase in kinetic energy is 0.003 MJ m^{-2} for the ECMWF model and 0.007 MJ m^{-2} for the E-model.

Comparing Figs. 3b and 5b we see that the main effect of truncation error on the predictions of the E-model is the production of a diffuse interface at the top of the mixed layer. Although the mixed layer is itself underestimated, the total region affected by convection extends to about 700 mb in the standard resolution case; i.e. about 80 mb (or one grid-level) deeper than that for the high-resolution case. This result is emphasized in Fig.6 which shows the fields of dT/dt for each case. Figure 6 also indicates that the high-resolution solution produces a steady increase in the mixed-layer depth during the daytime, while the standard-resolution case causes the depth to increase in bursts owing to the larger vertical grid size. Truncation error also leads to the dissipation of kinetic energy being overestimated by about 15% when the standard resolution is used. The surface transfer of sensible heat is underestimated by the standard-resolution case (1.58 MJ m^{-2} compared with 1.70 m^{-2} over 24 hrs), although the transfer of total heat across the surface is accurately predicted to be 2.10 MJ m^{-2} (cf 2.14 MJ m^{-2} for the high-resolution case). This occurs because the standard-resolution

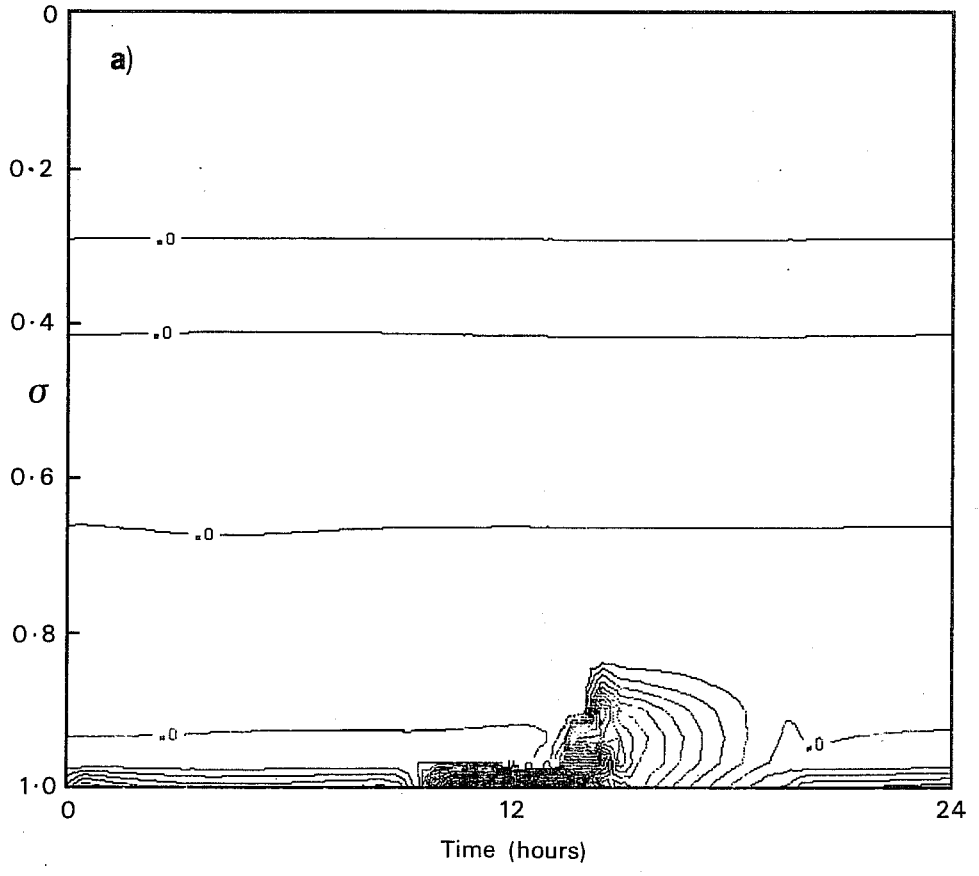

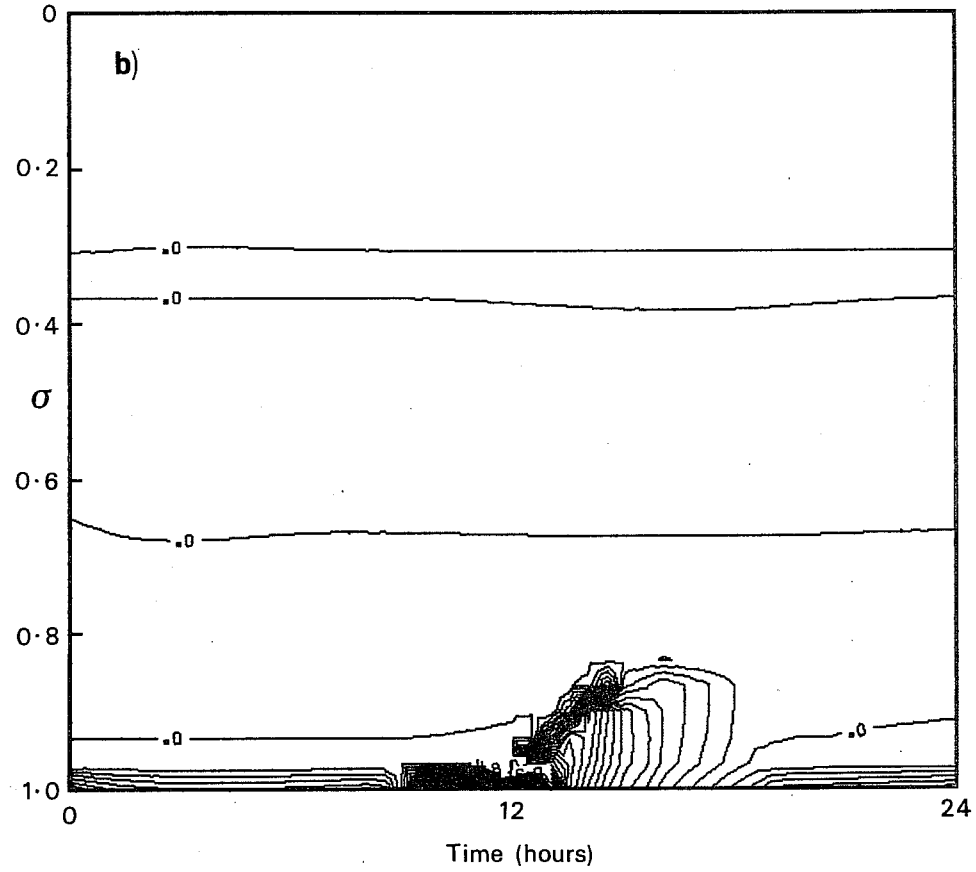

Fig. 6 Temporal variation of the rate of change of temperature dT/dt for Wangara conditions using the E-model; (a) N=15 and Δt=900s; (b)N=90 and Δt=225s.

case gives a mixed layer that is a little warmer and drier than the high-resolution case.

It is apparent from Figs.3 and 5 that the ECMWF model does not suffer from truncation error to the same extent as the E-model. Although the standard-resolution model does not yield a sharp well-mixed layer, Fig.7 shows that the depth of the boundary layer is accurately predicted. However, the intensity of the changes in T and q are somewhat underestimated near the top of the boundary layer in the standard-resolution case. Using the standard resolution we find that the transfer of sensible heat across the surface is only slightly underestimated (1.65 MJ m^{-2} rather than 1.71 MJ m^{-2} for 24 hrs) and the total heat transfer is 2.08 MJ m^{-2}, compared with 2.12 MJ m^{-2} for the high-resolution case. The dissipation of kinetic energy for the standard-resolution case is 0.058 MJ m^{-2}, which is 10% larger than the actual dissipation.

There is a continuing tendency to increase the spatial resolution of NWP models but at the same time to increase the integration time step Δt. We therefore show in Fig.8 the behaviour of q on the standard ECMWF grid when Δt is equal to 1350 s, which is currently used for the operational ECMWF spectral model. The representation of the mixed layer is apparently no worse in this case than when Δt is 900 s. However, the net transfers of both sensible and latent heat across the surface after 24 hrs are overestimated at 1.79 and 0.47 MJ m^{-2} respectively.

9. CONCLUSIONS

A parameterization of vertical diffusion, based on the turbulent energy model of Manton (1980), is compared with the results of the ECMWF scheme, which uses an explicit eddy diffusivity. Large-scale numerical models use large time

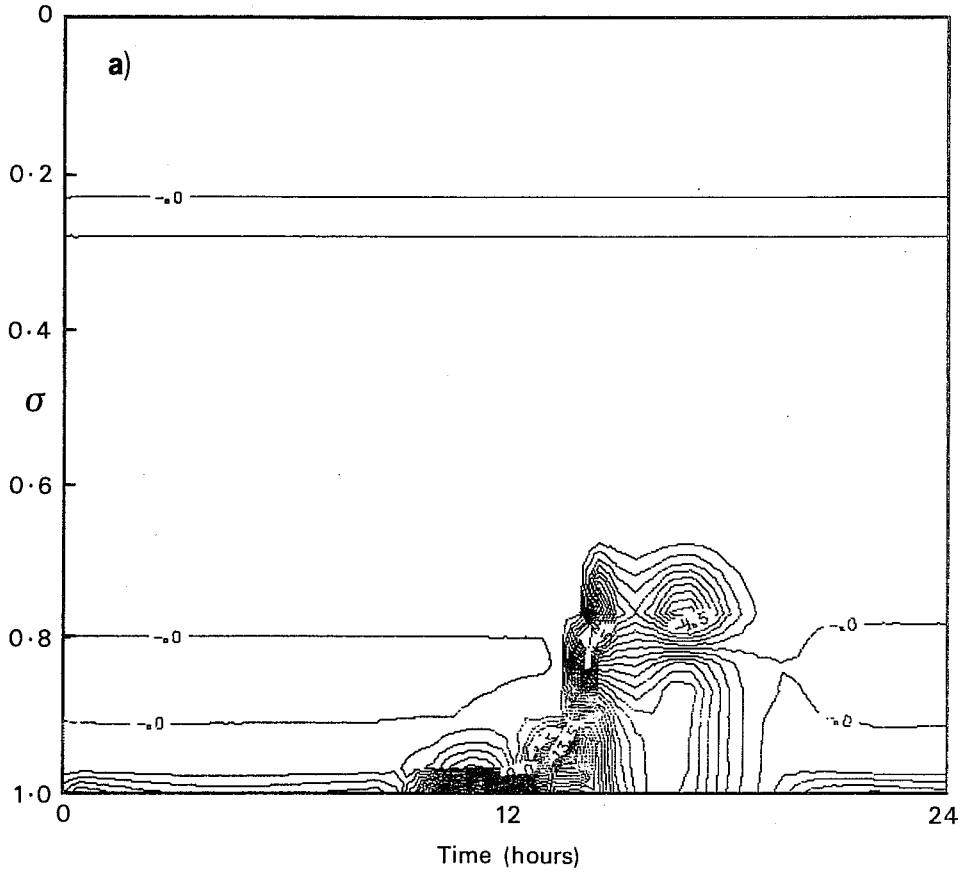

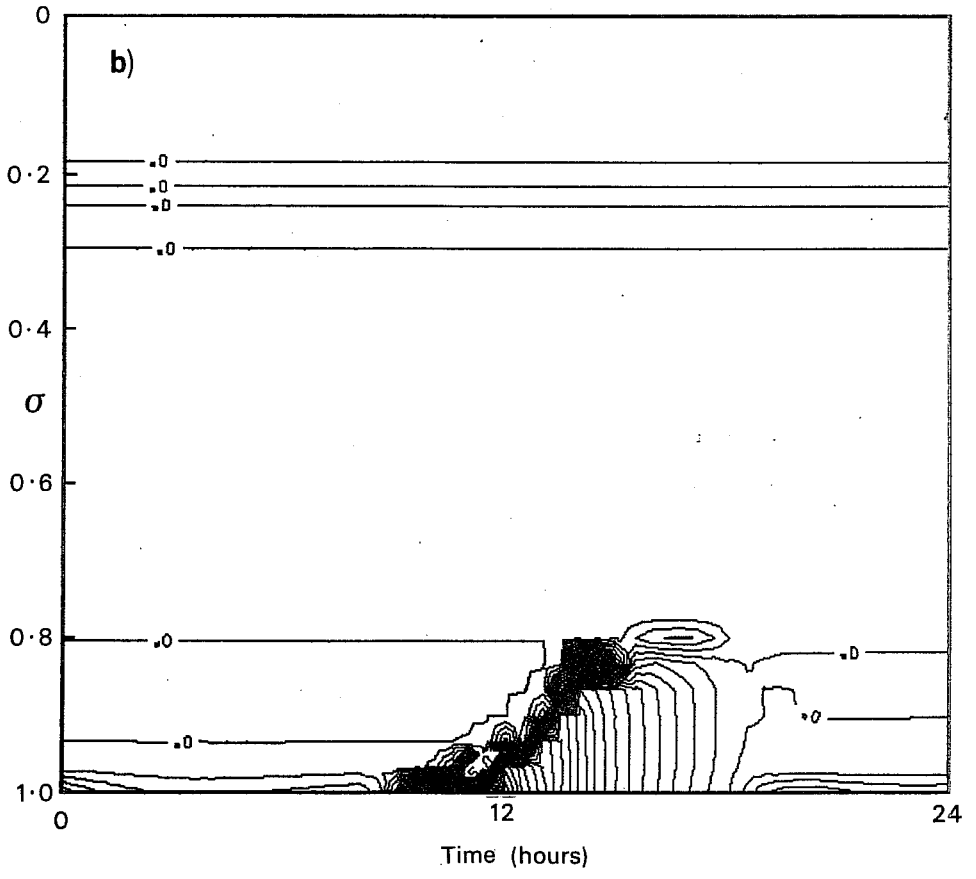

Fig. 7 Temporal variation of the rate of change of temperature dT/dt for Wangara conditions using the ECMWF model: (a)N=15 and Δt=900s; (b)N=90 and Δt=225s.

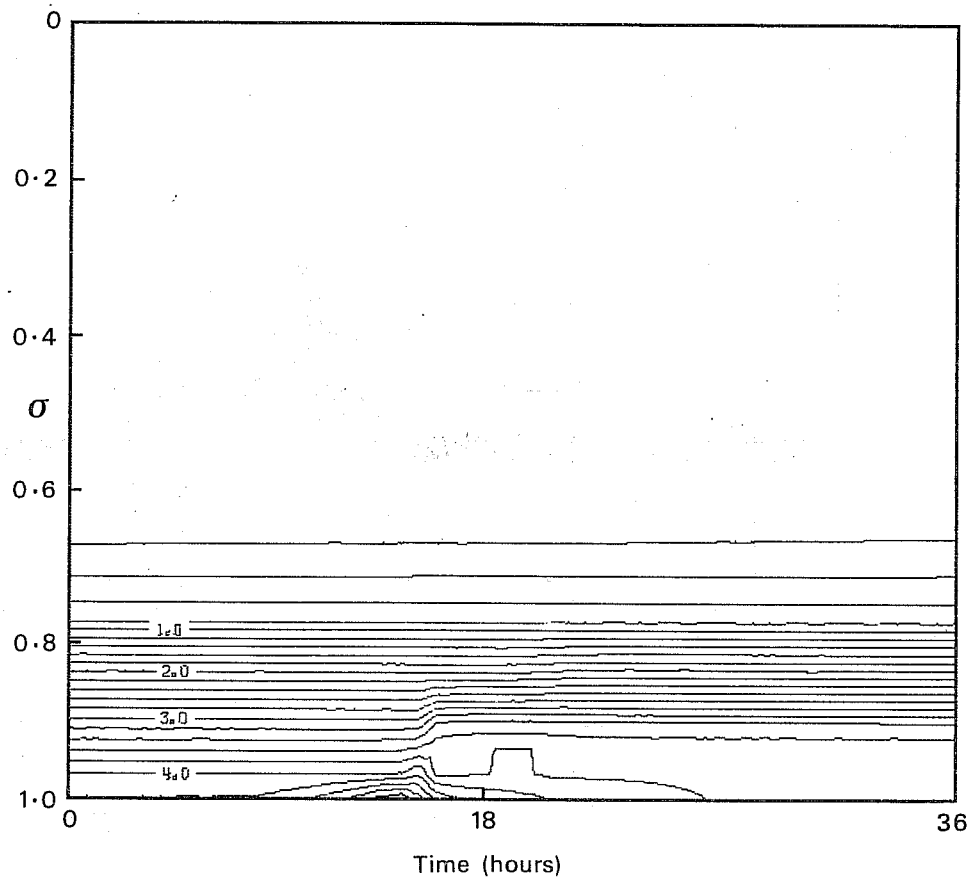

Fig. 8 Temporal variation of the water mass fraction q for Wangara conditions using the ECMWF model with the ECMWF grid with N=15 and Δt=1350s. Note that the time scale extends to 36 hrs.

steps that can be somewhat larger than the characteristic turbulent time scale. Hence the discretization of the equation for the turbulent energy E must be undertaken carefully. The tendency for E to approach its equilibrium value within the typical time step of NWP models suggests that, unless advection of E is found to be a dominant process, the value of E could be diagnosed at each time step.

The present E-model is found to give a reasonable estimate of the surface shear stress in near-neutral stability conditions, although the ECMWF model yields a better representation of the velocity profile. A comparison of the models over a diurnal cycle of the surface temperature shows that both models using high spatial resolution produce a sharp interface at the top of a well-mixed layer. However, the E-model produces a deeper convection layer than the ECMWF model. The extra entrainment causes the E-model mixed layer to be a little warmer and drier. On the other hand the net transfer of sensible and latent heat from the surface is the same for both models. This arises because the same parameterization of the fluxes in the surface layer is used in each case. The result also implies that the main impedance in the energy transfers between the troposphere and the surface occurs in the surface layer.

The deep convection layer generated by the E-model should allow it to extend the transfer of heat and moisture further into the tropical troposphere than does the ECMWF model. Although the behaviour of the models is generally similar near the surface, the ECMWF model dissipates kinetic energy over the whole atmosphere while dissipation in the E-model is restricted to the boundary layer. The net dissipation of kinetic energy is therefore much less in the E-model.

Spatial truncation error in both numerical models leads to excessive entrainment and so the mixed layer is a little too warm and dry when the vertical resolution is low. Consequently the transport of sensible heat across the surface is underestimated while the transport of latent heat is overestimated. Thus the net flux of energy at the surface is not greatly affected by spatial truncation error. A coarse spatial grid causes the dissipation of kinetic energy to be overestimated in the models. The present tests suggest that temporal truncation error is not excessive, except that the surface fluxes are overestimated for time steps greater than about 10^3 s.

Using the standard ECMWF spatial resolution (N=15 in (6.1)) in the E-model leads to truncation error such that the effects of the boundary layer extend about 80 mb (i.e. one grid level) deeper than they ought. The effects of truncation error are not so obvious in the ECMWF model, but the mixed layer with the standard resolution is not well-defined and the intensity of the changes in temperature and moisture is underestimated near the top of the boundary layer. Thus truncation error causes the ECMWF model to underestimate and the E-model to overestimate the transfer of heat, moisture amd momentum between the boundary layer and the middle levels of the troposphere.

References

Businger, J.A., Wyngaard, J.C., Izumi, Y. and Bradley, F.F. 1971: Flux-profile relationships in the atmospheric surface layer. J.Atmos.Sci. 28, 181-189.

Carson, D.J. and Smith, F.B. 1973: The Leipzig wind profile and the boundary layer wind-stress relationship. Quart.J.Roy.Met.Soc. 99, 171-177.

Clarke, R.H., Dyer, A.J., Brook, R.R., Reid, D.G. and Troup, A.J. 1971: The Wangara Experiment: Boundary Layer Data. CSIRO Div.Meteorol.Phys.Tech.Paper No.19.

Lettau, H. 1950: A re-examination of the "Leipzig Wind Profile" considering some relations between wind and turbulence in the friction layer. Tellus 2, 125-129.

Louis, J.-F. (ed) 1981: ECMWF Forecast Model Documentation Manual.

Louis, J.-F., Tiedtke, M. and Geleyn, J.-F., 1981: A short history of the operational PBL parameterization at ECMWF. Workshop on Planetary Boundary Layer Parameterization, ECMWF 59-79.

Manton, M.J. 1979: On the dispersion of particles in the atmosphere. Boundary-Layer Meteor. 17, 145-165.

Manton, M.J. 1980: On the modelling of mixed layers and entrainment in cumulus cloud. Boundary-Layer Meteor. 19, 337-358.

Mellor, G.L. and Yamada, T. 1974: A hierarchy of turbulence closure models for planetary boundary layers. J.Atmos.Sci. 31, 1791-1806.

Mildner, P. 1932: Uber die Reibung in einer speziellen Luftmasse in den untersten Schichten der Atmosphare. Beitr.Phys.Atmos. 19, 151-158.

Miyakoda, K. and Sirutis, J. 1977: Comparative integrations of global models with various parameterized processes of subgrid-scale vertical transport: description of the parameterizations. Contrib.Atmos.Phys. 50, 445-487.

Tiedtke, M. 1981: Assessment of the PBL-flow in the EC-model. Workshop on Planetary Boundary Layer Parameterization, ECMWF, 155-191.

Wyngaard, J.C. and Coté, O.R. 1971: The budgets of turbulent kinetic energy and temperature variance in the atmospheric surface layer. J.Atmos.Sci. 28, 190-201.

Wyngaard, J.C., Coté, O.R. and Izumi, Y. 1971: Local free convection, similarity, and the budgets of shear stress and heat flux. J.Atmos.Sci., 28, 1171-1182.

APPENDIX A - ONE-DIMENSIONAL BOUNDARY-LAYER MODEL

The one-dimensional model equations are taken to be

$$\frac{\partial u}{\partial t} = f\ (v-v_g) + \frac{1}{\rho}\frac{\partial}{\partial z}\ (\rho\ K_M \frac{\partial u}{\partial z}) + \dot{u}_a\ ,$$

$$\frac{\partial v}{\partial t} = f\ (u_g-u) + \frac{1}{\rho}\frac{\partial}{\partial z}\ (\rho\ K_M \frac{\partial v}{\partial z}) + \dot{v}_a\ , \qquad \text{(A1)}$$

$$\frac{\partial T}{\partial t} = \frac{1}{\rho}\frac{\partial}{\partial z}\ \{\rho\ K_Q\ \sigma^{Ra/Cpa}\ \frac{\partial}{\partial z}\ (T/\sigma^{Ra/Cpa})\} + \dot{T}_a + (L/Cpa)\ \dot{q}_\ell\ ,$$

$$\frac{\partial q}{\partial t} = \frac{1}{\rho}\frac{\partial}{\partial z}\ (\rho\ K_Q \frac{\partial q}{\partial z}) + \dot{q}_a - \dot{q}_\ell\ ,$$

where (u_g, v_g) is the (specified) geostrophic wind, f is the Coriolis frequency, T is the temperature, q in the mass fraction of water, $\dot{u}_a$, $\dot{v}_a$, $\dot{T}_a$ and $\dot{q}_a$ represent the (specified) adiabatic forcing of velocity, temperature and moisture, $\dot{q}_\ell$ is the rate of loss of water due to large-scale precipitation, and L is the latent heat of vaporization for water.

The adiabatic parts of (A1) are discretized by a centred time difference; for example, the increment δu_a in u due to adiabatic forcing is given by

$$\delta u_a = 2\Delta t\ \dot{u}_a\ . \qquad \text{(A2)}$$

The increments $(\delta u_g, \delta v_g)$ due to geostrophic forcing are given by the centred time-difference scheme

$$\delta u_g = 2\Delta t\ f\ (v^\tau - v_g)\ ,$$

$$\delta v_g = 2\Delta t\ f\ (u_g - u^\tau). \qquad \text{(A3)}$$

The increments in u,v,T and q due to vertical diffusion are found from the implicit scheme used in the ECMWF model; for example; the increment δq_v in q at the σ-level k is given by the equation

$$q^{\tau+1}_{*,k} - q^{\tau-1}_k = A_k\ (q^{\tau+1}_{*,k+1} - q^{\tau+1}_{*,k}) - C_k(q^{\tau+1}_{*,k} - q^{\tau+1}_{*,k-1})\ , \qquad \text{(A4)}$$

where $\delta q_v = q^{\tau+1}_{*,k} - q^{\tau-1}_k$;

A_k and C_k are defined in (4.3). Large-scale precipitation produces the increments δq_ℓ and δT_ℓ in q and T such that

$$\delta q_\ell = 0 = \delta T_\ell \text{ for } q^{\tau-1} + \delta q_a + \delta q_v \leq s ,$$

but if $q^{\tau-1} + \delta q_a + \delta q_v > s$ then

$$\delta q_\ell = s - (q^{\tau-1} + \delta q_a + \delta q_v) ,$$

$$\delta T_\ell = - (L/C_{pa})\, \delta q_\ell ; \tag{A5}$$

where s is the saturation mass fraction of water at temperture $T^{\tau-1} + \delta T_a + \delta T_v$. Using (A2) - (A5) we see that the values of the dependent variables, u,v,T and q at time $t = (\tau+1)\Delta t$ are given by

$$\begin{aligned} u^{\tau+1} &= u^{\tau-1} + \delta u_a + \delta u_g + \delta u_v , \\ v^{\tau+1} &= v^{\tau-1} + \delta v_a + \delta u_g + \delta v_v , \\ T^{\tau+1} &= T^{\tau-1} + \delta T_a + \delta T_v + \delta T_\ell , \\ q^{\tau+1} &= q^{\tau-1} + \delta q_a + \delta q_v + \delta q_\ell , \end{aligned} \tag{A6}$$

Equations (A1) - (A6) can be used to derive the terms in the budgets of kinetic energy K^τ, sensible heat P^τ and latent heat Q^τ at time τ, where

$$\begin{aligned} K^\tau &= \int \frac{1}{2} \rho(u^2 + v^2)dz = \sum_{k=1}^{N} \frac{1}{2} (p_s/g)(u^\tau\, u^{\tau-1} + v^\tau\, v^{\tau-1})\Delta\sigma_k , \\ P^\tau &= \int \rho\, C_{pa}\, T\, dz = \sum_{k=1}^{N} (C_{pa}\, p_s/g) T_k^\tau\, \Delta\sigma_k , \\ Q^\tau &= \int \rho\, L\, q\, dz = \sum_{k=1}^{N} (L\, p_s/g) q_k^\tau\, \Delta\sigma_k . \end{aligned} \tag{A7}$$

The rate of change of kinetic energy is found to be given by

$$(K^{\tau+1} - K^\tau)/2\Delta t = \sum_{k=1}^{N} \frac{1}{2} (p_s/g)\, (u_k^\tau\, \dot{u}_{a,k} + v_k^\tau\, \dot{v}_{a,k})\Delta\sigma_k$$

$$+ \sum_{k=1}^{N} \frac{1}{2} (p_s/g) f (v_k^{\tau} u_{g,k} - v_k^{\tau} v_{g,k}) \Delta\sigma_k$$

$$+ \sum_{k=1}^{N} \frac{1}{2} (p_s/g) (u_k^{\tau} \delta u_{v,k} + v_k^{\tau} \delta v_{v,k}) \Delta\sigma_k / 2\Delta t \ , \qquad \text{(A8)}$$

where the first term on the right-hand side of (A8) accounts for the work done locally by the adiabatic forcing, the second term is the work of the horizontal pressure gradient and the last term is the dissipation of energy. The equations for the rate of change of sensible and latent heat are

$$(P^{\tau+1} - P^{\tau-1})/2\Delta t = \sum_{k=1}^{N} (C_{pa}\, p_s/g) \dot{T}_{a,k}$$

$$+ (C_{pa}\, p_s/g)\, A_N\, (T_s - T_N^{\tau-1}/\sigma_N^{Ra/Cpa}) \Delta\sigma_N / 2\Delta t$$

$$- \sum_{k=1}^{N} (L p_s/g)\, \delta q_{\ell,k}\, \Delta\sigma_k \ , \qquad \text{(A9)}$$

$$(Q^{\tau+1} - Q^{\tau-1})/2\Delta t = \sum_{k=1}^{N} (L\, p_s/g) \dot{q}_{a,k}$$

$$+ (L\, p_s/g)\, A_N\, (q_s - q_N^{\tau-1}) \Delta\sigma_N / 2\Delta t$$

$$+ \sum_{k=1}^{N} (L p_s/g)\, \delta q_{\ell,k}\, \Delta\sigma_k \ , \qquad \text{(A10)}$$

where $q_s = W_s\, s\, (p_s, T_s) + (1 - W_s)\, q_N^{\tau-1}$;

the terms on the right-hand sides of (A9) and (A10) refer respectively to adiabatic forcing, surface fluxes and large-scale precipitation.

The numerical model can be run with up to 150 vertical levels on either a uniform grid or the ECMWF standard grid (6.1). The geostrophic wind and the adiabatic forcing terms are specified on the ECMWF grid with N=15. The surface values of pressure p_s, temperature T_s and wetness W_s are specified functions of time because no surface parameterization is provided in the model.

ECMWF PUBLISHED TECHNICAL REPORTS

No. 1 A Case Study of a Ten Day Prediction

No. 2 The Effect of Arithmetic Precisions on some Meteorological Integrations

No. 3 Mixed-Radix Fast Fourier Transforms without Reordering

No. 4 A Model for Medium-Range Weather Forecasting - Adiabatic Formulation

No. 5 A Study of some Parameterizations of Sub-Grid Processes in a Baroclinic Wave in a Two-Dimensional Model

No. 6 The ECMWF Analysis and Data Assimilation Scheme - Analysis of Mass and Wind Fields

No. 7 A Ten Day High Resolution Non-Adiabatic Spectral Integration: A Comparative Study

No. 8 On the Asymptotic Behaviour of Simple Stochastic-Dynamic Systems

No. 9 On Balance Requirements as Initial Conditions

No.10 ECMWF Model - Parameterization of Sub-Grid Processes

No.11 Normal Mode Initialization for a multi-level Gridpoint Model

No.12 Data Assimilation Experiments

No.13 Comparison of Medium Range Forecasts made with two Parameterization Schemes

No.14 On Initial Conditions for Non-Hydrostatic Models

No.15 Adiabatic Formulation and Organization of ECMWF's Spectral Model

No.16 Model Studies of a Developing Boundary Layer over the Ocean

No.17 The Response of a Global Barotropic Model to Forcing by Large-Scale Orography

No.18 Confidence Limits for Verification and Energetics Studies

No.19 A Low Order Barotropic Model on the Sphere with the Orographic and Newtonian Forcing

No.20 A Review of the Normal Mode Initialization Method

No.21 The Adjoint Equation Technique Applied to Meteorological Problems

No.22 The Use of Empirical Methods for Mesoscale Pressure Forecasts

No.23 Comparison of Medium Range Forecasts made with Models using Spectral or Finite Difference Techniques in the Horizontal

No.24 On the Average Errors of an Ensemble of Forecasts

No.25 On the Atmospheric Factors Affecting the Levantine Sea

No.26 Tropical Influences on Stationary Wave Motion in Middle and High Latitudes

ECMWF PUBLISHED TECHNICAL REPORTS

No.27 The Energy Budgets in North America, North Atlantic and Europe Based on ECMWF Analyses and Forecasts

No.28 An Energy and Angular-Momentum Conserving Vertical Finite-Difference Scheme, Hybrid Coordinates, and Medium-Range Weather Prediction

No.29 Orographic Influences on Mediterranean Lee Cyclogenesis and European Blocking in a Global Numerical Model

No.30 Review and Re-assessment of ECNET - a private network with Open Architecture

No.31 An Investigation of the Impact at Middle and High Latitudes of Tropical Forecast Errors

No.32 Short and Medium Range Forecast Differences Between a Spectral and Grid Point Model. An Extensive Quasi-Operational Comparison

No.33 Numerical Simulations of a Case of Blocking: The Effects of Orography and Land-Sea Contrast

No.34 The Impact of Cloud Track Wind Data on Global Analyses and Medium Range Forecasts

No.35 Energy Budget Calculations at ECMWF: Part I: Analyses

No.36 Operational Verification of ECMWF Forecast Fields and Results for 1980-1981

No.37 High Resolution Experiments with the ECMWF Model: A Case Study

No.38 The response of the ECMWF global model to the El-Nino anomaly in extended range prediction experiments

No.39 On the Parameterization of Vertical Diffusion in Large-Scale Atmospheric Models